Fresh Equatorial Jets

DEAN ROEMMICH, MICHELE MORRIS, AND W. R. YOUNG

Scripps Institution of Oceanography, La Jolla, California

J. R. DONGUY

ORSTOM/CSIRO, Hobart, Tasmania, Australia

(Manuscript received 8 June 1992, in final form 8 July 1993)

ABSTRACT

A vertically sheared eastward jet in the equatorial Pacific in late 1991 and early 1992 carried relatively fresh water from the western Pacific overriding the saltier surface layer of the central region. Salinity anomalies of about −1.0 psu were observed over a period of several months in a surface layer 50 m thick near the equator. Below this fresh layer there was a steep halocline having very little temperature stratification, so that the density changes were dominated by salinity. In December 1991, eastward surface velocities in the fresh jet at 170°W were 100 cm s^{-1} with a shear of about 40 cm s^{-1} in the top 100 m; the core of the jet was about 200 km in width, centered at 1.5°S. The jet decayed and vanished over the next few months, though the surface halocline remained.

A simple extension of the familiar 1½-layer model can account for the initial development of the sheared eastward jet. The surface pressure gradient in this initial value problem, tending to accelerate the fluid eastward, diminishes with depth because there is a zonal salinity gradient in the initially mixed layer. The depth dependence of the pressure gradient causes the accelerating flow to be vertically sheared, resulting in a tilting over of the isohalines. The shear progressively unmixes the mixed layer. The vertically integrated part of this solution is the Yoshida jet. The depth-dependent part of the solution results from a local conversion of potential to kinetic energy as the tilting isohalines lower the center of gravity of the surface layer. For added realism, generalizations of the model include wind forcing and a meridional salinity gradient.

While not discounting the conventional explanation of westerly wind stress in driving the eastward jet, it is shown that the tilting/shearing mechanism can be comparable to wind stress and is important in the production of salinity barrier layers. Fresh equatorial jets may provide a key to a better understanding of the physics of tropical ocean circulation and air–sea interaction during El Niño.

1. Introduction

Over most of the world's oceans, variations in surface-layer density are controlled principally by temperature, with salinity playing a secondary role. An interesting exception is in the western equatorial Pacific where, particularly in years preceding El Niño, a strong zonal gradient in salinity is found in a pool of very warm surface water with nearly uniform temperature. The salinity change is as large as 1 psu over a distance of 1000 km (Donguy and Morliere 1983) and is maintained by the very large westward increase in precipitation minus evaporation ($P - E$) in that region. Because of the substantial zonal contrast in surface density, the central equatorial waters may flow westward below the western surface waters or the western waters may flow eastward over the central. Either of these scenarios would create surface layers having small vertical temperature gradient, but with substantial layering in salinity and density. In the present work, some recent observations from the central Pacific illustrate a dramatic example of this phenomenon. Dynamical arguments demonstrate that the zonal salinity gradient is significant in driving the eastward surface jet and in the production of salinity layering.

Previous observations of surface waters with salinity layering (salinity barrier layers) in the western equatorial Pacific were described by Lukas and Lindstrom (1991). They showed an example at 155°E having a salinity increase of about 0.2 psu at 40 m depth. The corresponding temperature decrease of 0.2°C was sufficiently small that the density stratification was due mainly to salinity. It was suggested that such layers, acting to impede downward turbulent diffusion of heat, are important to the thermodynamics of air–sea interaction in the region. It was further hypothesized that they may play a role in the onset of El Niño.

McPhaden et al. (1992) described an eastward equatorial jet accompanied by salinity layering in late 1989 at 165°E. There the sheared jet was attributed to

Corresponding author address: Dr. Dean Roemmich, Scripps Institution of Oceanography, University of California, San Diego, 9500 Gilman Drive, La Jolla, CA 92093-0230.

westerly wind bursts that accompanied the eastward current, and the freshening of the surface layer to southward advection. During that episode the jet penetrated eastward only as far as the date line.

The present set of observations was collected in December 1991 through March 1992 in the central equatorial Pacific, near 170°W. Three meridional transects were carried out with closely spaced expendable bathythermograph (XBT) profiles and sparse expendable conductivity–temperature–depth (XCTD) profiles. At the time, oceanographic and meteorological conditions in the region indicated a mature El Niño, with a strong eastward oceanic surface jet centered south of the equator, weak zonal winds, frequent atmospheric convection, and a thick surface layer of water warmer than 29°C (Climate Analysis Center 1991b). XCTD profiles near the equator in all three transects had dramatic salinity barrier layers, with salinity stratification up to 1.0 psu and corresponding temperature stratification of only a few tenths of a degree.

In the following we begin with a description of the XBT/XCTD and surface velocity observations in 1991–92. Then some simple dynamical arguments are presented to show how shear in an eastward equatorial jet may be generated by a zonal salinity gradient in the surface layer. We do not dismiss the conventional explanation of westerly winds in driving the jet, but rather demonstrate that the zonal salinity gradient may be as important as the wind and can drive a sheared eastward jet in the absence of wind forcing. The dynamical solution is extended to include the effects of wind forcing and, for further realism, the existence of a meridional gradient in surface salinity. Finally, some speculative comments are made on the possible role of salinity in the evolution and propagation of El Niño events. The case for regular collection of salinity profiles in the equatorial oceans and for inclusion of salinity in coupled air–sea models is presented.

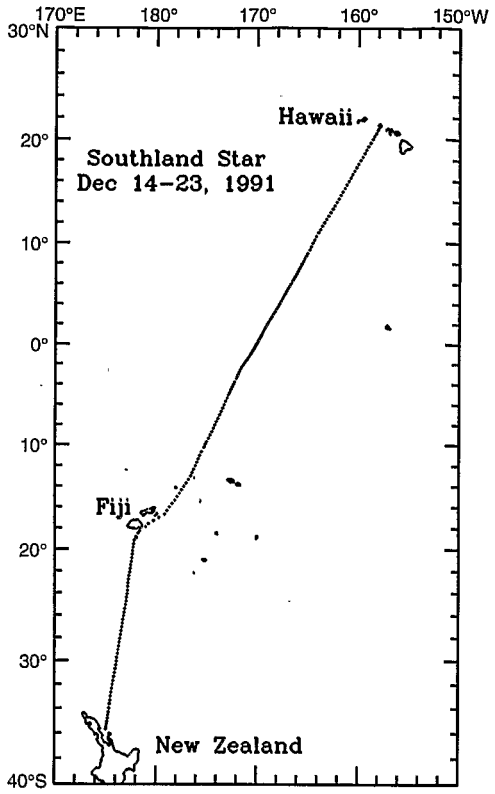

FIG. 1. Ship track of M/V *Southland Star* showing XBT locations in December 1991.

2. Observations

a. Temperature and salinity

As part of the World Ocean Circulation Experiment, high-resolution XBT transects have been obtained quarterly between New Zealand and Hawaii (Fig. 1) since 1987. Beginning in late 1991 XCTD profiles have also been collected from the same ship, M/V *Southland Star*. Mean pre-Niño temperature along the New Zealand–Hawaii track, from the average of 15 cruises between September 1987 and July 1991, is shown in Fig. 2a. A pool of warm surface water above 29°C extends from 5° to 10°S. A temperature minimum is seen on the equator and vertical spreading of isotherms in the equatorial thermocline indicates the eastward velocity maximum of the equatorial undercurrent. The temperature distribution is very similar to that constructed by Kessler and Taft (1987) from XBT data along the central Pacific track. An estimate of the mean salinity field is shown in Fig. 2b. This is constructed from the measured mean temperature field by using a *T–S* correlation, varying with latitude along the track of *Southland Star*. The *T–S* relation is estimated from historical hydrographic data in the NODC archive. The surface salinity maximum in the South Equatorial Current at about 5°S in Fig. 2b separates fresher surface waters to the north and south. Surface waters fresher than 35 psu at 11°S and north of 3°N mark the eastward flowing South Equatorial Countercurrent and North Equatorial Countercurrent, respectively.

In December 1991, 95 XBTs and 8 XCTDs were dropped between 16°S and 6°N (Fig. 3), as part of the longer transect. Transects are designated by year and month, for example, 9112 for December 1991. The heavily sampled temperature section strikingly shows the effects of El Niño when compared to the mean temperature (Fig. 2a). The southern pool of surface water warmer than 29°C has grown substantially, crossing the equator to 5°N. The surface temperature minimum on the equator, indicative of equatorial upwelling, is missing. The top of the thermocline is displaced downward with sharpened vertical temperature gradient. There is no evidence of the Equatorial Undercurrent. Another notable feature in Fig. 3 is the considerable shoaling of the thermocline ridge, which

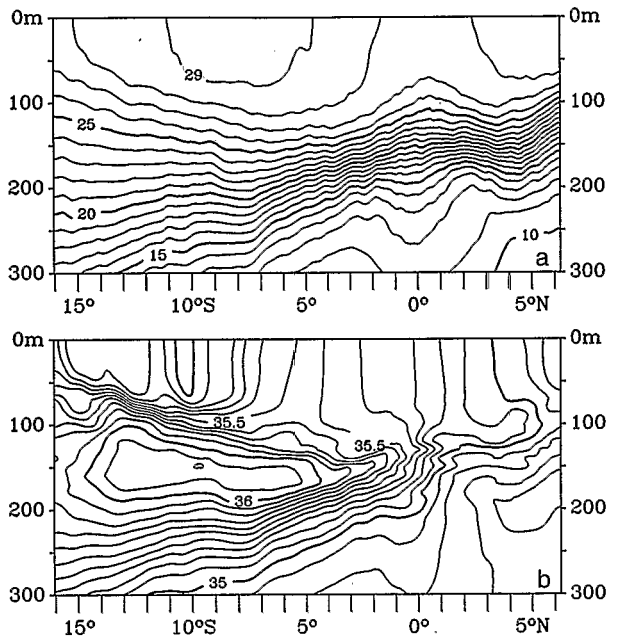

FIG. 2. (a) Mean temperature in the top 300 m from 15 high-resolution XBT transects during mid-1987 to mid-1991. (b) Estimate of mean salinity constructed from temperature using a T–S relation. The T–S relation varies with latitude alongtrack and is estimated from hydrographic data in the NODC archive.

is located at about 10°S. That ridge is the southern edge of the South Equatorial Countercurrent.

Voyage 9112 was the first in the program having XCTD probes—indeed, it was the first deployment of XCTDs from any Pacific merchant vessel. Salinity in the top 300 m is shown in Fig. 3 (lower). To emphasize the variation of salinity in the pool of warm surface water, the region having temperature greater than 29°C has been shaded. The surface salinity maximum at 5°S is narrowed and diminished in magnitude with respect to the mean salinity (Fig. 2b). A pool of anomalously fresh surface water extends across the equator from the north.

Individual temperature and salinity profiles near the equator in voyage 9112 (Fig. 4) display a thick surface layer, with sea surface temperatures about 29.6°C, decreasing very gradually to 29.2°C at about 115 m. Below that, in the very sharp upper thermocline, the temperature drops by 10° in the next 30 to 40 m. XCTD profiles at 1°28′S, 0°2′N, and 2°38′N all showed large salinity gradients (barrier layers) within the nearly isothermal layer of 29°C water (Fig. 4). The former of these has a salinity increase of 1.0 psu, occurring mostly between 50 and 70 m depth, near the center of the warm layer. The corresponding density increase of 8 $\times 10^{-4}$ g cm^{-3} between the ocean surface and 115 m (from σ_θ equals 21.5 to 22.3) is dominated by salinity. For comparative purposes, this amounts to about 15% of the density change through the thermocline. With respect to historical hydrographic data near the same location, the salinity in the top 50 m was anomalously fresh by 0.9 psu at 1°28′S. The salinity anomaly decreased to zero near the base of the 29°C layer. Outside of the equatorial band, XCTD profiles at 4°13′S and 6°20′N had no significant salinity gradients in the surface layer (Fig. 4). Farther south, other XCTD profiles showed increasing salinities through the isothermal layer, but the magnitudes of salinity change were lower, about 0.2 psu, and without the sharp gradients seen in the equatorial profiles.

In the next voyage, in late January and early February 1992 (voyage 9201), the equatorial barrier layer was again observed (Fig. 5). Now the temperature was even more uniform; temperature variation was less than 0.03° from the ocean surface to 135 m depth. The fresh surface layer was thicker and the salinity increased from 34.6 psu to 35.0 psu between 80 and 100 m. Unfortunately, there were only 4 XCTD probes available for this voyage and 2 had wire breaks above 100 m. The temperature distribution (Fig. 6) showed a greatly diminished pool of 29°C water, split into two bands. The equatorial band of warm water was centered just north of the equator.

During voyage 9203, 11 XCTDs were dropped. Barrier layers were not found south of the equator (Fig. 7) and surface salinities south of the equator had returned to values near 35 psu. But at the equator and to the north the barrier layers were once again observed (Fig. 7). The equatorial warm pool was further dimin-

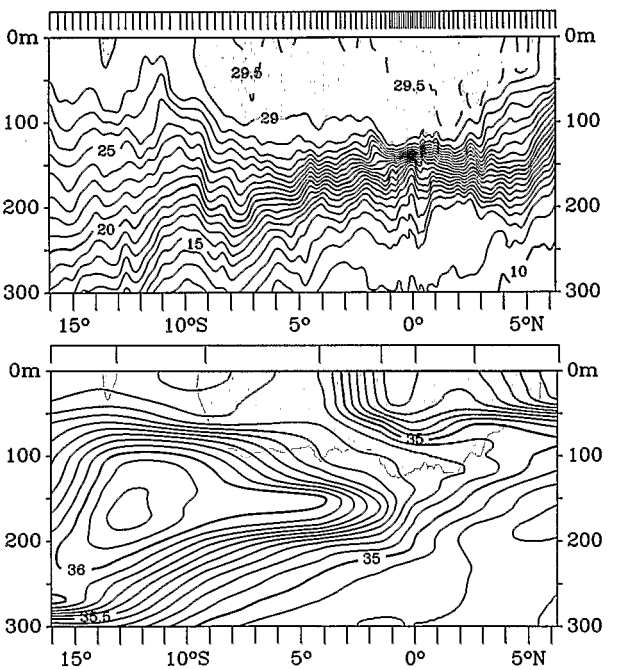

FIG. 3. XBT temperature (upper panel) and XCTD salinity (lower panel) sections, December 1991. Shading on the salinity section indicates water warmer than 29°C. Tick marks above each panel indicate probe locations.

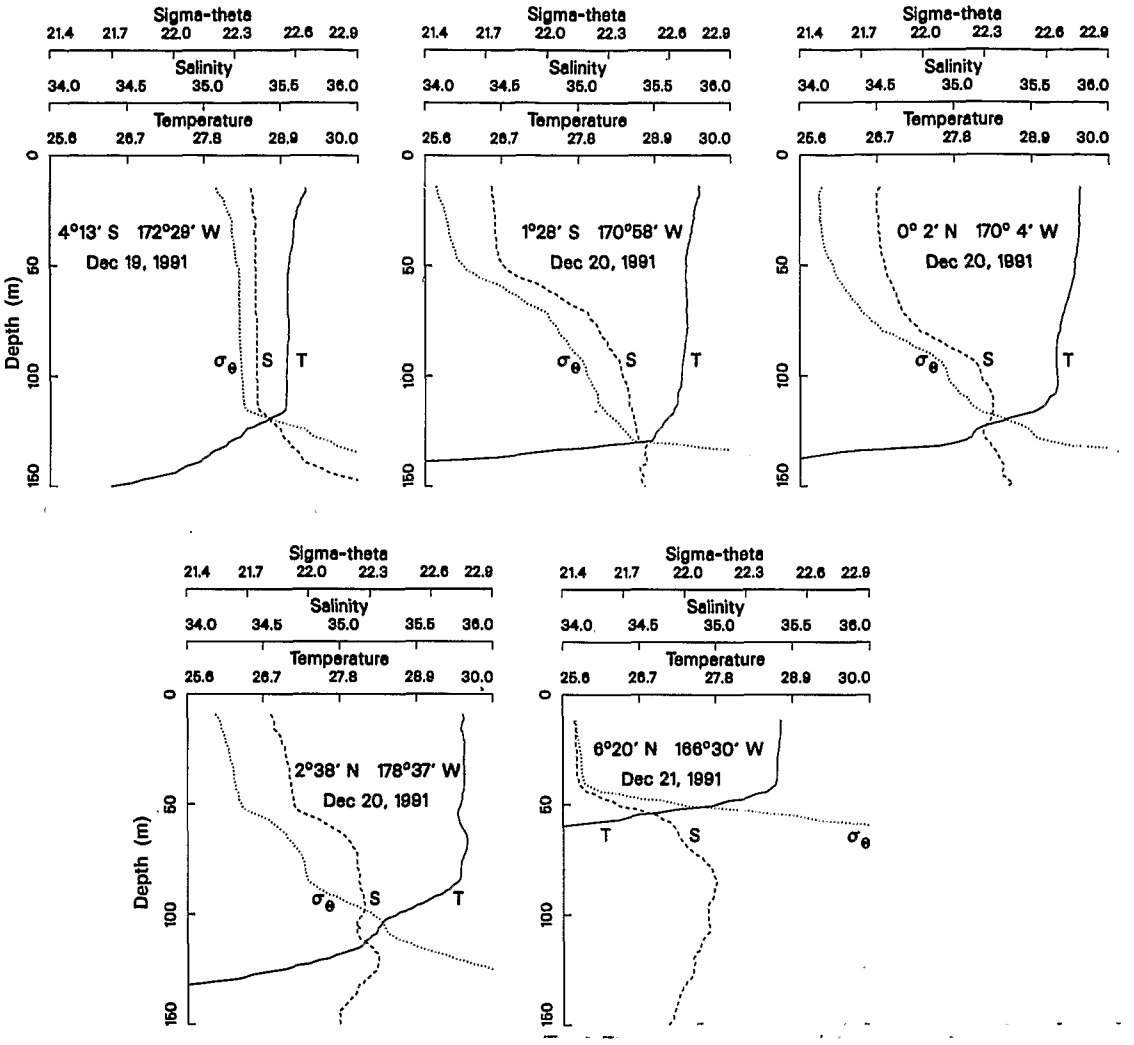

FIG. 4. XCTD profiles of temperature, salinity, and sigma-theta, December 1991. Horizontal scaling is chosen so that horizontal offsets in temperature or salinity produce equivalent offsets in sigma-theta.

ished and still centered north of the equator (Fig. 8). The sharp meridional gradient in salinity has been displaced from about 2°S in voyage 9112 to the equator in voyage 9203. It is still associated with the diminished equatorial pool of 29°C water.

b. *Velocity*

Three different techniques are used to obtain a description of the velocity field. (i) Surface currents are calculated from ship drift. (ii) Geostrophic velocity is estimated from the XBT/XCTD data. (iii) About 20 surface drifters from the TOGA/WOCE surface velocity program, carried eastward in the equatorial jet (Bi and Niiler 1994, personal communication), help to define the spatial and temporal characteristics of the jet. About 8 of these crossed 170°W during the study period.

During the *Southland Star* transects, the across-ship component of ocean surface current is estimated from ship drift using a GPS navigation system to obtain the ship's velocity. The ship's gyrocompass/autopilot system is used for heading information. Set is calculated from the difference between the heading and displacement vectors and is then corrected for windage to estimate ocean surface current. Principal errors in this calculation are due to both gyro and windage corrections. Daily estimates of gyro error from sextant observations suggest gyro drifts of less than 1°, resulting in a velocity error of 20 cm s^{-1}. The windage error can be of the same order in moderate winds, though during voyage 9112 it was absolutely calm through the equatorial band. The ship does not have a sufficiently accurate speed log to permit estimation of the component of drift along track.

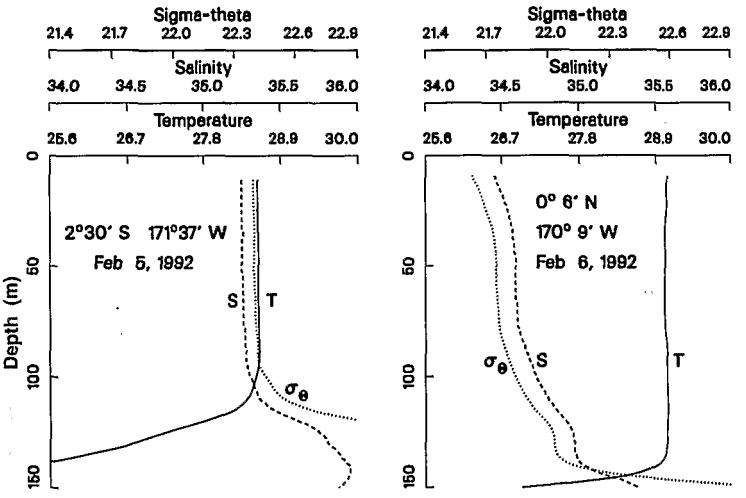

FIG. 5. XCTD profiles of temperature, salinity, and sigma-theta, February 1992. Horizontal scaling as in Fig. 4.

Surface current estimates from ship drift in voyage 9112 are shown in Fig. 9. The individual estimates are made from 15-minute intervals of GPS data, corresponding to averaging of about 8 km along track. GPS measurement error, estimated from the apparent drift of a stationary GPS antenna, is typically less than 5 cm s^{-1} over 15-minute intervals. The ship drift shows two eastward jets, one at 7° to 9°S and the other at about 2°S. The former is the eastward flowing South Equatorial Countercurrent, but is unusually strong for that feature. The latter is in the band normally occupied by the westward South Equatorial Current. Maximum speed is about 100 cm s^{-1}.

In addition to the ship drift calculation, Fig. 9 also shows an estimate of geostrophic surface current relative to 800 db. This estimate was made using the high resolution temperature data (Fig. 2a), together with a *T–S* relation derived from interpolation of historical and XCTD data to estimate specific volume. This technique probably underestimates shear in the top 100 m in salinity barrier layers because it cannot reproduce the large salinity stratification at nearly constant temperature. As an alternative we have also estimated geostrophic velocity from objective mapping of the XCTD temperature and salinity profiles alone. The spatial resolution is crude, but the geostrophic shear in the top 100 m, associated with the sharply sloping isohalines at about 1°30′S, is roughly 40 cm s^{-1}. Interestingly, Fig. 9 shows good qualitative agreement between the geostrophic surface velocities (from XBT and *T–S* relation) and surface ship drift velocities. Both show the maxima in eastward flow at 2° and 9°S. During voyage 9201 these maxima were reduced but still present. In voyage 9203 the eastward jet was no longer seen. Instead, a strong westward surface flow had appeared just north of the equator.

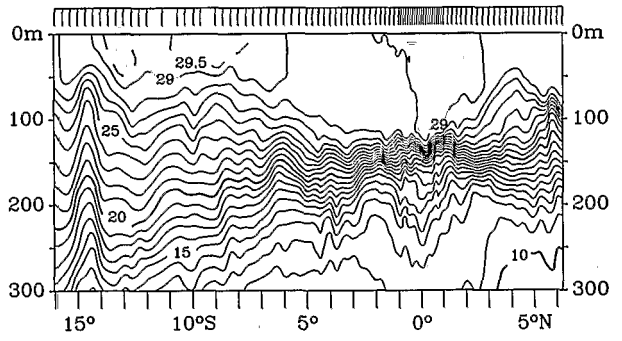

FIG. 6. XBT temperature section, late January–early February 1992. Tick marks indicate probe locations.

Further confirmation of the anomalous eastward flow field is given by surface drifting buoys shown in Fig. 10 [adapted from Bi and Niiler (1994, personal communication)]. Drifters showed eastward flow between 10°S and 10°N in December and January in the central and western Pacific. The jet first appeared in surface drifter tracks in the western equatorial Pacific in August 1991, and then moved progressively eastward to about 140°W in February 1992. Figure 10 is a composite of tracks of the 20 drifters entrained in the eastward jet during this interval. Eastward velocities were as high as 130 cm s^{-1} over 10-day intervals. In addition to the strong eastward flow, there was some southward displacement of the drifters with long zonal tracks.

In summary, measurements at about 170°W in late 1991 indicated an anomalously broad and deep pool of water warmer than 29°C containing a strong salinity barrier layer at 50–70 m depth in profiles near the equator. The salinity barrier layer, with anomalous salinity stratification as high as 1 psu, was associated with a strong eastward surface jet. Eastward velocities of about 100 cm s^{-1} were seen in ship drift calculations,

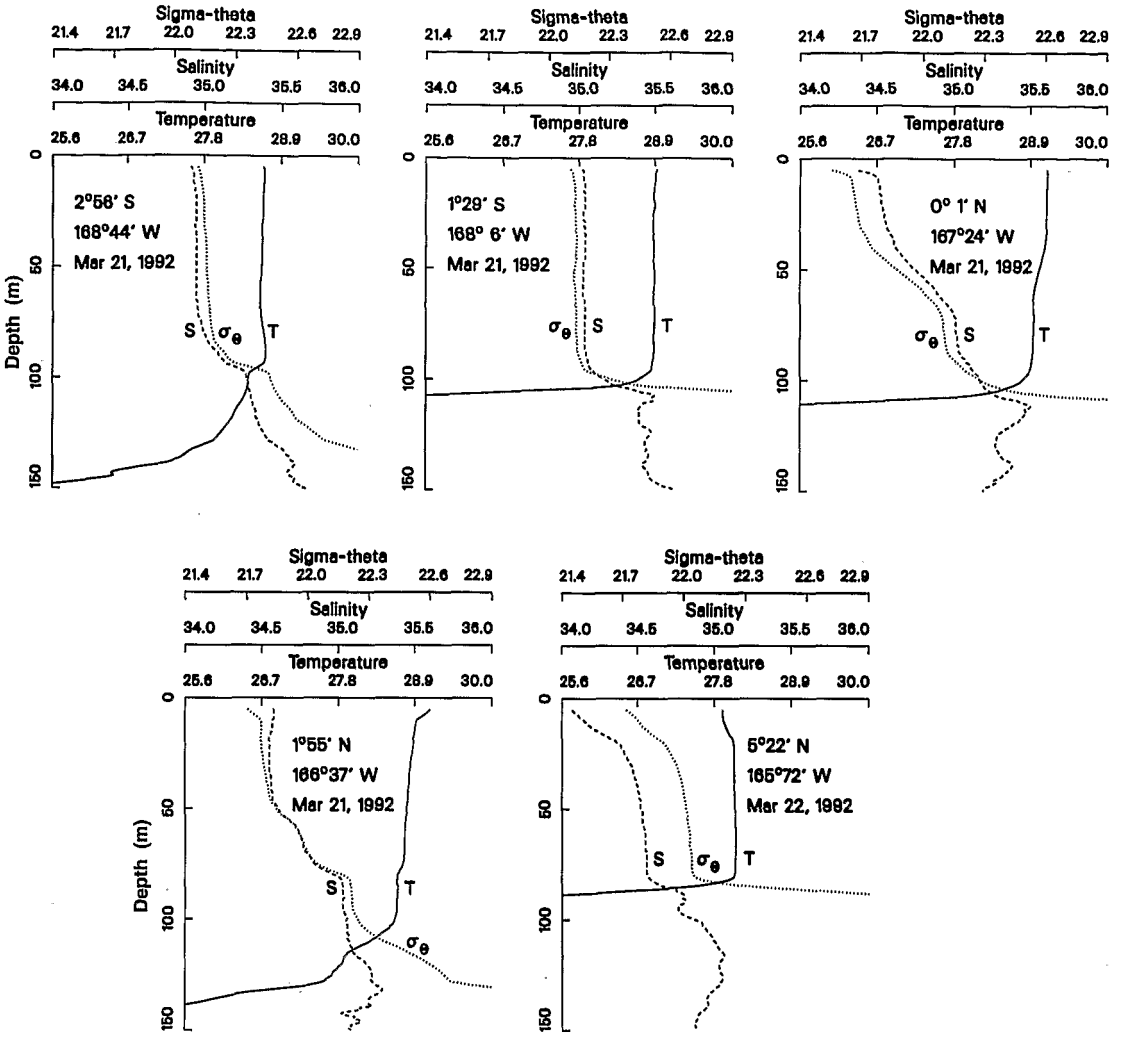

FIG. 7. XCTD profiles of temperature, salinity, and sigma-theta, March 1992. Horizontal scaling as in Fig. 4.

geostrophic shear calculations and surface drifter trajectories, in place of westward flow associated with the South Equatorial Current. The meridional scale of the surface jet was about 200 km and the jet was displaced south of the equator at about 1°30'S. The jet had weakened in January 1993 and was absent by March. Surface drifter trajectories indicated that some water parcels traveled thousands of kilometers eastward, originating in the relatively fresh waters of the western equatorial Pacific and eventually crossing 170°W. Aside from zonal advection of freshwater, meridional advection and local rainfall may have also contributed to the observed fresh anomalies.

3. Dynamics

a. What drives the eastward jet; why is there a barrier layer?

Here we will consider the relative importance of westerly wind stress, zonal sea surface slope, and zonal salinity gradients in driving the eastward jet. The former involves a direct transfer of kinetic energy to the ocean surface layer, the latter two are conversions of potential to kinetic energy, the potential energy having been previously contributed by the trade winds and by thermohaline forcing in the form of a zonal gradient in precipitation minus evaporation ($P - E$). The importance of the ($P - E$) forcing mechanism is perhaps less apparent than the other two. But scaling arguments demonstrate that all three can be comparable (and any one may dominate locally) and furthermore that the thermohaline mechanism may help to explain some aspects of the observations that cannot easily be attributed to other causes.

Eastward equatorial surface jets have been documented in the last three El Niño episodes. Firing et al. (1983) measured eastward surface flows in excess of 130 cm s^{-1} in late 1982 on the equator near 160°W. The flow was vertically sheared, with an eastward velocity of 40 cm s^{-1} at 140 m. McPhaden et al. (1990)

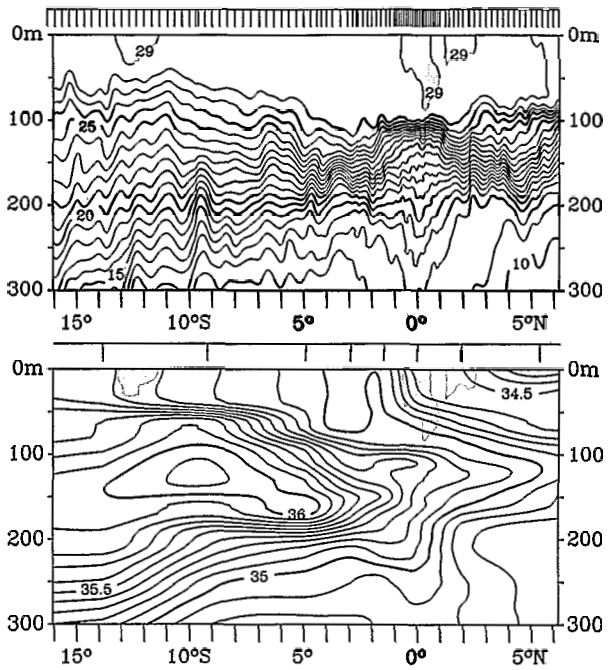

FIG. 8. XBT temperature (upper panel) and XCTD salinity (lower panel) sections, March 1992. Shading on the salinity section indicates water warmer than 29°C. Tick marks indicate probe locations.

described prolonged eastward surface flows at 165°E during late 1986 and mid-1987. The eastward equatorial jet has also been observed in the western equatorial Pacific in non–El Niño years, for example, by Inaba at 160°E in January 1989 (Lukas 1990) and by McPhaden et al. (1992) at 165°E in late 1989.

The equatorial jets have previously been modeled as the response of the upper ocean to anomalous westerly wind stress (e.g., Philander 1990). The eastward jet at 165°E in late 1989 (McPhaden et al. 1992), was clearly associated with westerly winds. Eastward stresses were up to about 0.5 dyn cm^{-2} on the equator for periods of 1 to 2 weeks (McPhaden et al. 1992, Fig. 4), accompanied by eastward surface flows up to 1 m s^{-1}. In later 1991, the equatorial Pacific west of the date line had weak wind stress with periods of moderate westerlies. Because the region normally has moderate easterly tradewinds, the resulting westerly anomaly in wind stress was substantial (roughly 0.5 dyn cm^{-2}, Climate Analysis Center 1991a,b). Lacking easterly stress to balance the zonal pressure gradient, the mixed layer accelerates eastward. In the simplest models, an accelerating surface layer of constant density is considered, lying over a deep layer at rest. Hydrostatic balance guarantees that the zonal pressure force is independent of depth, z, in the mixed layer and therefore that the resulting acceleration is also uniform with depth.

Now consider a more realistic elaboration of the mixed layer, in which the density of the mixed layer, $0 > z > -h(x, y, t)$, is independent of z, but does vary horizontally. In that case the acceleration varies with z. Specifically, suppose that the density in the mixed layer is represented as

$$\rho = \rho_0[1 - g^{-1}b(x, y, t)], \tag{1}$$

where $b(x, y, t)$ is the buoyancy. As shown in Fig. 11, we suppose that ρ_0 is the density of fluid below the mixed layer so that static stability requires $b > 0$. For simplicity we use a linear approximation to the equation of state:

$$b = g[\alpha_T(T - T_0) - \alpha_S(S - S_0)], \tag{2}$$

where $T_0 = 12°$ and $S_0 = 35$ psu are the temperature and salinity of the fluid below the mixed layer. For the fluid in the mixed layer we take $T = 29.5 \pm 1/2$°C and $S = 35 \pm 1/2$ psu. Since $\alpha_T = 3.3 \times 10^{-4}(°C)^{-1}$ and $\alpha_S = 7.5 \times 10^{-4}$ $(psu)^{-1}$ the reduced gravity at the base of the mixed layer produced by the 17.5° drop in temperature is 5.66 cm s^{-2}. The vertical salinity difference makes a negligible contribution to the reduced gravity. However, in anticipation of a more detailed discussion below, we emphasize that for lateral variations of density within the mixed layer the reverse is true: the 1 psu variations in salinity produce larger lateral buoyancy variations than the 1° variations in temperature.

From the hydrostatic relation we can calculate the pressure distribution in the mixed layer as

$$p(x, y, z, t) = -\rho_0 gz + \rho_0 b(x, y, t)z + p_S(x, y, t), \tag{3}$$

where the surface pressure, $p_S(x, y, t)$, is the constant of integration. The usual 1 1/2-layer assumption is that the pressure gradient below $z = -h$ is much less than the pressure gradient above $z = -h$. Now the pressure field below $z = -h$ (where the density is just ρ_0) is

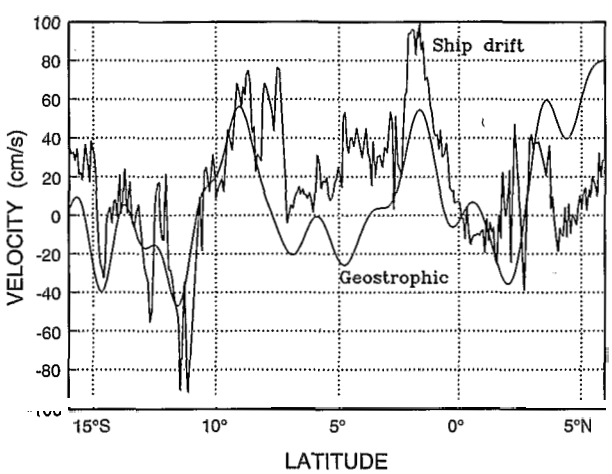

FIG. 9. Surface geostrophic velocity and across-track (Fig. 1) ship drift velocity during December 1991 plotted as a function of latitude. Positive values indicate eastward flow.

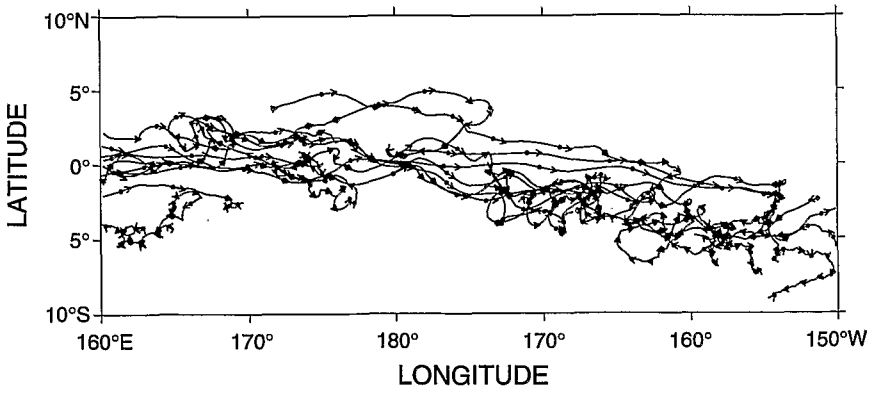

FIG. 10. Daily averaged drifter trajectories from July to the end of February, adapted from Bi and Niiler (1994, personal communication). Arrows are drawn every ten days on each track.

$$p = -\rho_0(bh + gz) + p_S. \quad (4)$$

If the gradient of the deep pressure field in (4) vanishes, then $\nabla p_S = \rho_0 \nabla bh$. Thus, if the displacement of the free surface from the geoid is denoted by ζ, then

$$p_S = \rho_0 g\zeta = \rho_0 bh. \quad (5)$$

Using the relation above we can express the gradient of the shallow ($0 > z > -h$) pressure in (3) in terms of h and b. Thus, if $0 > z > -h$,

$$\nabla p = \rho_0 z \nabla b + \nabla p_S = \rho_0 \nabla[b(z + h)], \quad (6)$$

where $\nabla = (\partial_x, \partial_y)$.

If b is a constant, as in the standard 1½-layer model, then (6) reduces to a well-known result: b is just the reduced gravity and the acceleration due to the pressure gradient is independent of z and proportional to ∇h. However, if $\nabla b \neq 0$ then the acceleration due to the horizontal pressure gradient depends on z. For instance, the pressure gradient at the surface is

$$\nabla p(x, y, 0, t) = \rho_0 \nabla bh = \rho_0 b \nabla h + \rho_0 h \nabla b, \quad (7)$$

while the pressure gradient at the base of the mixed layer is

$$\nabla p(x, y, -h, t) = \rho_0 b \nabla h. \quad (8)$$

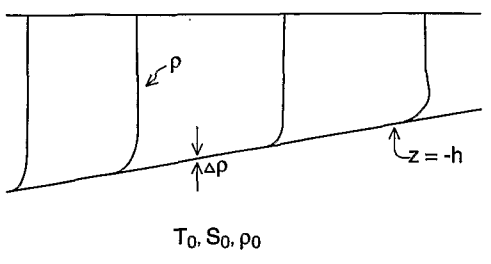

FIG. 11. A schematic of the density structure in the active layer. The fluid below the active layer has temperature $T_0 = 12°C$ and salinity $S_0 = 35$ psu.

In the equatorial Pacific close to the date line, $h_x < 0$ and $b_x \approx -g\alpha_S S_x < 0$ so that p_x is negative at both the surface and the base of the mixed layer. However, this eastward acceleration is larger at the surface because b_x and h_x in (7) are both negative.

As a simple thought experiment, imagine that the zonal pressure gradient at all depths in the mixed layer is initially balanced by turbulent stresses produced by a westward surface wind stress. If the wind turns off then the resulting unbalanced pressure gradient will produce an eastward acceleration at all depths. But the acceleration is a maximum at the surface and as a result relatively fresh water from the west moves eastward faster at $z = 0$ than it does at $z = -h$. This process of sheared eastward acceleration is illustrated in Fig. 12. The initially vertical isopycnal surfaces are tilted over zonally and as a result the mixed layer is progressively unmixed. We propose this tilting as a mechanism for the production of salinity barrier layers at the onset of El Niño. In section B we reinforce the "tendency argument" given above with a more complete dynamical argument.

To assess the relative importance of the zonal buoyancy gradient in producing vertically sheared zonal acceleration, we estimate the acceleration at the sea sur-

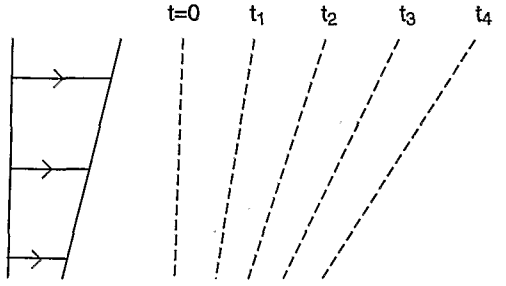

FIG. 12. A schematic illustration of tilting mechanism. The vertically sheared acceleration differentially advects the initially vertical isohaline surfaces. As a result fresh water from the west moves eastward faster at the surface than at the base of the active layer.

face and the difference between this and the acceleration at the base of the mixed layer. Estimates of mean dynamic topography indicate an upward sea surface slope of roughly 10 dyn cm between 170°W and about 170°E, with the sea surface flattening farther to the west (Wyrtki 1984). In late 1991, island sea level gauges indicated eastward propagation of a sea level height anomaly (Climate Analysis Center 1991a,b). This may have enhanced the eastward drop in surface height by an additional 10 cm. The accelerating sea level change is therefore estimated as $\Delta\zeta \approx 10$ to 20 cm over $L = 2000$ km, yielding an acceleration of $g\Delta\zeta/L \approx 5 \times 10^{-5}$ to 10×10^{-5} cm s^{-2}.

Between the ocean surface and the base of the mixed layer the acceleration is reduced in proportion to the zonal buoyancy gradient [compare (7) with (8)]. In the years preceding El Niño, the western equatorial Pacific has a large zonal gradient in sea surface salinity. A composite of pre–El Niño years by Donguy and Morliere (1983) shows equatorial surface salinities of about 34.3 psu at 140°E, increasing to about 35.5 psu at the date line. The zonal gradient appears to be as high as about 1 psu per 1000 km and the position of the high gradient region fluctuates zonally during the year. The high zonal gradient in surface salinity is attributable to the high gradient in precipitation minus evaporation ($P - E$), more than 2.5 m yr^{-1} in annual average $P - E$ between 170°W and 150°E (Donguy 1987). Maps of measured sea surface salinity (SSS) in October 1991 and February 1992 are shown in Fig. 13. These months provided the best spatial coverage of SSS in the ORSTOM volunteer ship salinity program. Unfortunately, coverage was poor in December. The October map clearly shows a high zonal gradient in SSS just east of the date line. The main difference between this map and the composite October pre–El Niño map of Donguy and Morliere (1983) is that the region of high zonal salinity gradient was located farther to the east in October 1991. Because of the large separation between ship tracks, coverage is not sufficient to resolve the detailed structure of the SSS field but the maximum in zonal gradient appears to be at least 1 psu over 2000 km. The corresponding zonal temperature gradient was small. SST analyses in late 1991 (Climate Analysis Center 1991a,b) showed a large pool of water warmer than 29°C occupying the entire western equatorial region. Temperature changes were a degree or less over several thousand kilometers. Using $h = 100$ m, $dS/dx = 1$ psu 2000 km and $dT/dx = 0$, the reduction in acceleration between the ocean surface and the base of the mixed layer is 4×10^{-5} cm s^{-2}. Thus, because of the zonal salinity gradient, the acceleration at the base of the mixed layer is only 40% to 80% of that at the ocean surface.

Both the acceleration due to sea surface slope and the vertical change in acceleration due to the zonal salinity gradient are of order 5×10^{-5} cm s^{-2}. How does this compare to acceleration by wind stress? A

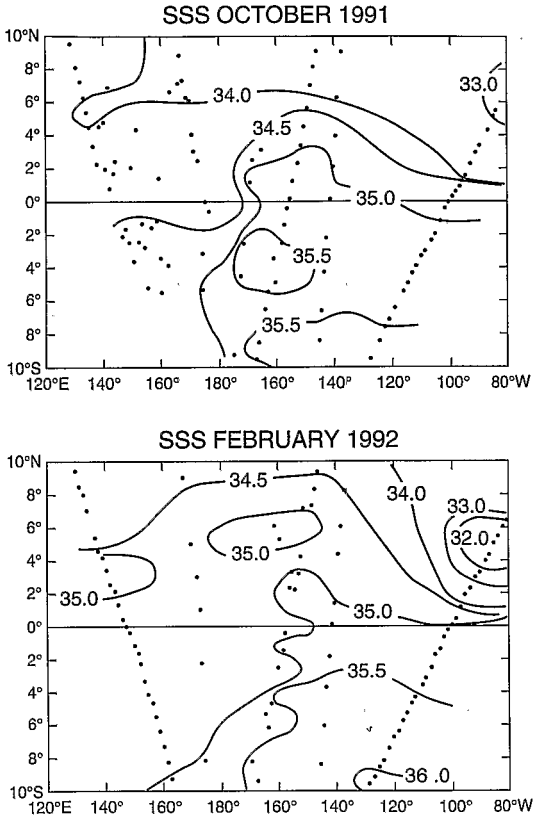

FIG. 13. Maps of sea surface salinity (SSS) from the ORSTOM volunteer ship program. The upper panel is from October 1991 and the lower panel is from February 1992.

stress of 0.5 dyn cm^{-2} acting on a mixed layer 20 m thick produces an acceleration of 2.5×10^{-4} cm s^{-2}. But if the resultant momentum is mixed down to 100 m, then the acceleration and shear are of the same order as in sea surface slope/zonal salinity gradient estimates given above. It is therefore concluded that in those regions where the zonal salinity gradient is high, the tilting/shearing mechanism is significant. The specific role of westerly winds in driving the eastward jet during 1991–92 is discussed by Bi and Niiler (1994, personal communication).

The tilting/shearing mechanism indicates that the strongest tendency for barrier layer creation will occur at the longitude of highest zonal salinity gradient. Then, the barrier layers are carried eastward by the vertically averaged eastward velocity within the surface layer. Because the initial zonal salinity gradient is locally concentrated, rather than linear (Fig. 11, 13), the resulting barrier layer profile will have a steep vertical gradient, much as was observed (Fig. 4) in the central Pacific.

The scaling arguments given above are valid only during the initial, accelerating phase of the jet. If a denotes the acceleration then the advective time scale for this accelerating jet is $(L/a)^{-1/2}$, or about 20 days. This leads to velocities of order 100 cm s^{-1}, which is comparable to the observed velocities. During this time, surface waters

will have moved eastward about 1000 km, with perhaps half that displacement at the base of the surface layer.

For times longer than 20 days, the problem becomes far more complicated. Acceleration diminishes as frictional forces begin to balance the zonal pressure gradient. The tilting and shearing may produce instabilities leading to mixing across the developing halocline. Using the scales mentioned above, the gradient Richardson number is about 2 for the surface layer as a whole. For long times, rainfall becomes an important source of buoyancy at the ocean surface. The highly convective region moved eastward in late 1991, more or less synchronously with the eastward jet (Climate Analysis Center 1991a,b). With rainfall rates of about 50 cm mo^{-1}, this is enough fresh water to dilute a layer 50 m thick by 1 psu in 3 months. On the long time scale there may be both erosion of the barrier layer by mixing and reinforcement by rainfall. The arrival of high atmospheric convection at 170°W does not appear to have occurred early enough to account for the barrier layer in December 1991 but could account for the freshness by the following March. Another possibility is that the low salinity cap could be produced by southward advection. The drifter observations (Fig. 10) show some southward tendency in addition to the strong zonal flow. The model addresses this contribution by inclusion of a meridional as well as a zonal gradient in salinity (Appendix).

The observations we have described above and illustrated in Figs. 3–10 are undoubtedly a product of the longer time scale with all of its complexities. The surface drifters (Fig. 10) indicated that the eastward jet began around August in the western Pacific and decayed around February. Our observations span several months and began several months after the jet first appeared. The tilting/shearing mechanism cannot account for the complexity of the fully developed jet seen in the observations. But the tendencies and the spatial and temporal scales imposed in the accelerating phase persist and are highly consistent with the XBT/XCTD and velocity datasets described in the previous section.

b. The Yoshida jet and the fresh jet

We now formulate a model of the vertically sheared eastward acceleration described in section 3a. Our point of departure is the equatorial β-plane equations for a Boussinesq fluid. The density is represented as in (1) and (2), and the remaining equations of motion are

$$\frac{Du}{Dt} - \beta yv + \rho_0^{-1}p_x = \rho_0^{-1}\sigma_z, \tag{9a}$$

$$\frac{Dv}{Dt} + \beta yu + \rho_0^{-1}p_y = \rho_0^{-1}\tau_z, \tag{9b}$$

$$-b + \rho_0^{-1}p_z = 0, \tag{9c}$$

$$u_x + v_y + w_z = 0, \tag{9d}$$

$$\frac{Db}{Dt} = 0. \tag{9e}$$

The convective derivative is $D/Dt \equiv \partial_t + u\partial_x + v\partial_y + w\partial_z$ and (σ, τ) is the vertical Reynolds stress.

The equations above apply in the active region, which is $0 > z > -h(x, y, t)$. We now introduce the notation

$$\tilde{\theta}(x, y, t) \equiv \theta(x, y, -h, t), \tag{10}$$

and assume that the surface of density discontinuity at $z = -h$ is also a material surface. This means that on the time scales of interest there is no entrainment of fluid into the active layer. Using the notation in (10) this condition can be written as

$$h_t + \tilde{u}h_x + \tilde{v}h_y + \tilde{w} = 0, \tag{11}$$

or equivalently

$$h_t + \left(\int_{-h}^{0} u dz\right)_x + \left(\int_{-h}^{0} v dz\right)_y = 0. \tag{12}$$

In (9), p is the deviation of the pressure from the static profile in the deep layer, where the density is ρ_0. Thus in the active layer, $0 > z > -h(x, y, t)$, the total pressure field is

$$P = -\rho_0 gz + p. \tag{13}$$

The assumption that the pressure gradients vanish below $z = -h$ is then seen to be equivalent to

$$\tilde{p} = 0. \tag{14}$$

This is a boundary condition at $z = -h(x, y, t)$ on the system in (9).

For orientation it is helpful to first consider the special case where $\nabla b(x, y, z, 0) = 0$. Then from (9e) the buoyancy is constant for all time. Integrating (9c) and applying the boundary condition in (14) gives $p = \rho_0 b(z + h)$. Thus the pressure gradient in (9a) and (9b) is independent of z and the constant buoyancy, b, is the "reduced gravity." Since the pressure gradient is independent of z the resulting velocity fields are also independent of z and (12) is $h_t + (uh)_x + (vh)_x = 0$. Thus, we recover the usual shallow-water equations when $\nabla b = 0$ at $t = 0$.

It is also easy to verify that (9) has an energy conservation law:

$$\mathcal{E}_t + \nabla \cdot \mathcal{F} = \rho_0^{-1}(u\sigma_z + v\tau_z), \tag{15}$$

where

$$\mathcal{E} \equiv \frac{1}{2}(u^2 + v^2) - bz, \quad \mathcal{F} \equiv (\mathcal{E} + \rho_0^{-1}p)\mathbf{u}. \tag{16}$$

If (15) is integrated vertically we find

$$\partial_t \int_{-h}^{0} \mathcal{E}\, dz + \partial_x \int_{-h}^{0} u(\mathcal{E} + \rho_0^{-1}p)dz + \partial_y \int_{-h}^{0} v(\mathcal{E} + \rho_0^{-1}p)dz = \tilde{w}\tilde{p} + \int_{-h}^{0} \rho_0^{-1}(u\sigma_z + v\tau_z)dz. \tag{17}$$

Because of (14) the source term $\tilde{w}\tilde{p}$ on the right-hand side of (17) is zero. The form above emphasizes that the boundary condition in (14) isolates the active layer from interaction with the fluid below $z = -h$.

We now suppose that when $t < 0$ the density field has the form

$$b = B(1 - \Gamma_B x), \quad h = H(1 - \Gamma_H x). \tag{18}$$

For simplicity we suppose that the meridional stress and meridional pressure gradient are zero. Further, when $t < 0$, the pressure, $p = \rho_0 B(1 - \Gamma_B x)[z + H(1 - \Gamma_H x)]$, has a zonal gradient that is balanced by the stress divergence: $p_x = \sigma_z$. Thus all of the velocities are zero when $t < 0$. Notice that because the zonal pressure gradient, p_x, depends linearly on z the usual "slab Ekman layer" assumption, namely, that σ_z is independent of z, is not valid. Instead one must assume that $\sigma_z(x, y, z, t < 0)$ is precisely the linear function of z that is required to balance $p_x(x, y, z, t < 0)$ at every point.

The ultimate source of the stress divergence, σ_z, is the easterly wind at the surface. If at $t = 0$ the wind switches off, or reverses sign and becomes eastward, then there is an unbalanced pressure gradient that accelerates the fluid eastward. To solve this problem we must simplify (9) and the necessary approximations are best made in dimensionless variables.

Using B and H from (18), we define the dimensional scales

$$c^2 \equiv BH, \quad R \equiv \sqrt{c/\beta}, \quad T \equiv 1/\sqrt{c\beta}. \tag{19}$$

Here c is the Kelvin wave speed and with $H = 10^4$ cm and $B = 5.6$ cm s^{-2} we find $c = 237$ cm s^{-1}; R is the equatorial deformation radius. With $\beta = 2.27 \times 10^{-13}$ (cm s)$^{-1}$ we have $R = 323$ km. The time scale T is then $T = 1.36 \times 10^5$ s or 37.9 h.

The familiar equatorial scaling is

$$(x, y) = R(\hat{x}, \hat{y}), \quad z = H\hat{z}, \quad t = T\hat{t},$$
$$(u, v) = c(\hat{u}, \hat{v}), \quad w = (H/R)c\hat{w}, \; p = \rho_0 c^2 \hat{p},$$
$$b = B\hat{b}, \quad h = H\hat{h}, \quad \sigma = \rho_0 (H/R) c^2 \hat{\sigma}_0. \tag{20}$$

With these definitions the nondimensional equations are

$$\frac{Du}{Dt} - yv + p_x = \sigma_z, \tag{21a}$$

$$\frac{Dv}{Dt} + yu + p_y = 0, \tag{21b}$$

$$-b + p_z = 0, \tag{21c}$$

$$u_x + v_y + w_z = 0, \tag{21d}$$

$$\frac{Db}{Dt} = 0. \tag{21e}$$

Here we have dropped the hats and written the equations of motion when $t > 0$ so that the meridional stress term is zero and σ_0 is a steady eastward wind. The remaining conditions are the nondimensional versions of (11) and (14), namely,

$$\tilde{p} = 0, \quad h_t + \tilde{u}h_x + \tilde{v}h_y + \tilde{w} = 0. \tag{22}$$

The first nondimensional parameter in the theory is the zonal length scale. We are focusing on an equatorial strip 2000 km long and thus, using a centered coordinate system, the nondimensional domain is $-L/2 < x < L/2$, where $L \approx 6.2$. The other nondimensional parameters in the problem come from scaling the initial conditions in (18). In nondimensional variables we have

$$b(x, y, z, t < 0) = 1 - \epsilon_B x,$$
$$h(x, y, z, t < 0) = 1 - \epsilon_H x,$$
$$p(x, y, z, t < 0) = (1 - \epsilon_B x)[z + 1 - \epsilon_H x],$$
$$\sigma_z(x, y, z, t < 0) = p_x(x, y, z, t < 0), \tag{23a–d}$$

where the nondimensional zonal gradients are

$$\epsilon_H = R\Gamma_H, \quad \epsilon_B = R\Gamma_B. \tag{24}$$

As the notation suggests, the nondimensional gradients are small. Specifically, if the depth of the mixed layer at the eastern end of the domain is 90 m and the depth at the western end is 110 m, then $\epsilon_H \approx 0.032$. And if the salinity varies by 1 psu over this same 2000 km excursion, then $\epsilon_B \approx 0.022$. (Note that since the domain length is 6.2 the fractional variation in buoyancy from one end to the other is about 0.13 or 0.14. This small fraction is the ratio of the buoyancy change due to 1 psu zonal increase in salinity divided by the buoyancy change due to a 17.5° vertical drop in temperature.)

The linear variation in buoyancy in (23a) is not very realistic. A better model would compress the 1 psu salinity change into a distance of about 1000 km, for example, $b = 1 - \epsilon_B \tanh(kx)$ with $k \approx 1$ or 1.5. However, the simplicity of the following calculation is lost if this more elaborate initial condition is adopted.

We reiterate that when $t < 0$, the slab Ekman layer assumption does not apply: from (23c) and (23d) it is clear that σ_z is a linear function of z when $t < 0$. But we now assume that at $t = 0$ the surface stress, σ_0, reverses sign and becomes positive. Further, we suppose that the divergence associated with this stress is uniformly distributed throughout the mixed layer. Thus $\sigma_z(x, y, z, t > 0) = \sigma_0 > 0$, so that at $t = 0$ the zonal momentum equation is suddenly subjected to two unbalanced eastward forces: the preexisting zonal pressure gradient in (23c) and the stress divergence associated with the eastward wind stress.[1]

[1] The reader may have noticed that while we do not use the slab Ekman layer assumption when $t < 0$, we do so when $t > 0$. At the cost of notational elaboration it is straightforward to encompass the possibility of a nonslab stress divergence when $t > 0$. For example, take $\sigma_z(x, y, z, t > 0) = \sigma_0[1 + \gamma(z + 1/2)]$, where γ is a free parameter so that the slab case is recovered when $\gamma = 0$. Since there are no firm constraints on γ, this additional complication is not included in our theory.

We take advantage of the small parameters by defining

$$\epsilon \equiv \sqrt{\epsilon_H \epsilon_B}, \quad \mu = \sqrt{\epsilon_B/\epsilon_H}, \tag{25}$$

and then expanding in ϵ with μ fixed and of order unity. Specifically

$$\begin{aligned}(u, v, w) &= \epsilon(u_1, v_1, w_1) + \epsilon^2(u_2, v_2, w_2) + \cdots \\ b &= 1 - \epsilon\mu x + \epsilon b_1 + \epsilon^2 b_2 + \cdots \\ h &= 1 - \epsilon\mu^{-1}x + \epsilon h_1 + \epsilon^2 h_2 + \cdots .\end{aligned} \tag{26}$$

The initial conditions are that $u_1 = v_1 = w_1 = h_1 = b_1 = 0$.

One very important simplification is immediately apparent. The first two orders in the expansion of (21e) are

$$b_{1t} = 0, \quad b_{2t} = \mu u_1. \tag{27}$$

From the initial conditions we conclude that $b_1 = 0$. Thus the expansion of the pressure field is

$$p = 1 + z + \epsilon[h_1 - \mu^{-1}x - \mu x(1 + z)] + O(\epsilon^2). \tag{28}$$

The order ϵ balances in the remaining equations of motion are

$$\begin{aligned}u_{1t} - yv_1 - \mu(1 + z) - \mu^{-1} + h_{1x} &= \sigma_0, \\ v_{1t} + yu_1 + h_{1y} = 0, \quad h_{1t} + \bar{u}_{1x} + \bar{v}_{1y} &= 0,\end{aligned} \tag{29a–c}$$

where we have used the notation

$$\bar{\theta} \equiv \int_{-1}^{0} \theta dz,$$

$$\theta(x, y, z, t) = \bar{\theta}(x, y, t) + \theta'(x, y, z, t). \tag{30}$$

We shall refer to the vertically averaged fields, such as $\bar{u}_1$, as the "barotropic" part of the flow, while the remainder, u'_1, is "baroclinic."

To solve (29) we first observe at this first order the solution is independent of x: $h_{1x} = u_{1x} = 0$, etc. Then we vertically average the remaining equations to get

$$\begin{aligned}\bar{u}_{1t} - y\bar{v}_1 &= (\mu/2 + \mu^{-1} + \sigma_0), \\ \bar{v}_{1t} + y\bar{u}_1 &= -h_{1y}, \\ h_{1t} + \bar{v}_{1y} &= 0.\end{aligned} \tag{31}$$

The solution of (31) is a well-known problem in equatorial oceanography, namely, the "Yoshida jet." Thus, we have

$$\begin{aligned}\bar{u}_1 &= (\mu/2 + \mu^{-1} + \sigma_0)y^{-1}\mathcal{Q}''(y)t + u_1^{\dagger}(y, t), \\ \bar{v}_1 &= (\mu/2 + \mu^{-1} + \sigma_0)\mathcal{Q}(y) + v_1^{\dagger}(y, t), \\ h_1 &= -(\mu/2 + \mu^{-1} + \sigma_0)\mathcal{Q}'(y)t + h_1^{\dagger}(y, t),\end{aligned} \tag{32}$$

where the function $\mathcal{Q}(y)$ is the bounded solution of

$$\mathcal{Q}'' - y^2\mathcal{Q} = y. \tag{33}$$

The fields $u_1^{\dagger}(y, t)$ etc. are required because the Yoshida jet does not satisfy $v_1(x, y, 0) = 0$. Explicit expressions for $u_1^{\dagger}$, etc. are given by Moore and Philander (1977). These fields are inertial oscillations excited by the abrupt switch-off of the wind and we ignore them in the following discussion.

Subtracting (31) from (29) one finds a closed set of equations for the baroclinic part of the velocity field. Specifically

$$\left.\begin{aligned}u'_{1t} - yv'_1 &= \mu(z + 1/2) \\ v'_{1t} + yu'_1 &= 0\end{aligned}\right\}. \tag{34}$$

The solution is

$$\left.\begin{aligned}u'_1 &= \mu t(z + 1/2)\left[\frac{\sin\xi}{\xi}\right] \\ v'_1 &= -\mu t(z + 1/2)\left[\frac{1 - \cos\xi}{\xi}\right]\end{aligned}\right\}, \tag{35}$$

where

$$\xi \equiv yt. \tag{36}$$

The velocities in (35) have no vertically integrated transport ($\overline{z + 1/2} = 0$), so they do not induce a vertical velocity at $z = -1$ and do not move the lower boundary. Changes in depth of the mixed layer are produced solely by the barotropic fields $\bar{u}_1$ and $\bar{v}_1$ in (32). It is remarkable that the baroclinic and barotropic problems decouple so cleanly. This simplicity is a consequence of (27a) and is not a property of the higher-order terms in the expansion.

The baroclinic velocities in (35) are not affected by the surface wind stress because of the slab Ekman layer assumption in (29a), that is, the stress divergence appears as a uniform body force, σ_0, rather than a function of z. Consequently, the baroclinic velocities in (35) are due solely to the horizontal buoyancy gradient and the resultant sheared acceleration. It is likely that wind stress also plays a part in producing the observed velocity shear. Incorporating this physics into our model presents no conceptual difficulties but would force us to confront the longstanding issue of how to parameterize turbulent stresses. Here it is our intention to show that the strong buoyancy gradient near the date line is sufficient to produce sheared accelerations, and hence form barrier layers, even if the westerly wind forcing is zero. The solution in (35) makes this essential point and shows that it does not rest on parameterizations of turbulent mixing.

The velocities in (35) are vertically sheared inertial oscillations. The limit $y \to 0$ is peculiar because the inertial frequency is zero at the equator. Thus, as we show below in (40), the zonal velocity on the equator accelerates linearly with time. But the meridional width

of this zonal jet narrows as $1/t$ so that the total zonal transport of the baroclinic flow is independent of time:

$$\int_{-\infty}^{\infty} u_1'(y, t)dy = \pi\mu(z + 1/2). \quad (37)$$

[Note that the result above is not inconsistent with the initial condition $u_1'(y, 0) = 0$: if y is fixed and $t \to 0$ then from (35) we see that $u_1'(y, t) \to 0$.]

Using linear superposition the solution of (29) is the sum of the fields in (32) and (35). Thus, the complete vertical velocity is

$$w_1 = -(\mu/2 + \mu^{-1} + \sigma_0)\mathcal{Q}'(y)z + \frac{\mu t^2}{2}\left[\frac{\xi \sin\xi - 1 + \cos\xi}{\xi^2}\right](z + z^2). \quad (38)$$

From (27b) we can now calculate

$$b_2 = \left(\frac{\mu^2 t^2}{2}\right)(\mu/2 + \mu^{-1} + \sigma_0)y^{-1}\mathcal{Q}''(y) + \mu^2 t^2\left[\frac{1 - \cos\xi}{\xi^2}\right](z + 1/2). \quad (39)$$

The velocities in (32), (35), and (38) are not singular at the equator. Specifically if we take the limit $y \to 0$, we find the leading-order structure at the equator is

$$u_1(0, z, t) = [(\mu/2 + \mu^{-1} + \sigma_0) + \mu(z + 1/2)]t$$

$$v_1(y, z, t) = -y[0.6(\mu/2 + \mu^{-1} + \sigma_0) + (\mu t^2/2)(z + 1/2)]$$

$$w_1(0, z, t) = 0.6(\mu/2 + \mu^{-1} + \sigma_0)z + (\mu t^2/4)(z + z^2)$$

$$b_2(0, z, t) = \frac{\mu t^2}{2}[(\mu/2 + \mu^{-1} + \sigma_0) + \mu(z + 1/2)]. \quad (40)$$

(We have used $\mathcal{Q}'''(0) = 1$ and $\mathcal{Q}'(0) = -\sqrt{\pi} \times \Gamma(3/4)/\Gamma(1/4) \approx -0.6$, where $\Gamma(z)$ is the Gamma function.) Thus, on the equator, both the barotropic and baroclinic zonal velocities accelerate linearly with time. Using our earlier estimates for ϵ_H and ϵ_B, we find that $\mu \approx 0.8$. Then from (40a) the velocity at the base of the mixed layer is about 60% of the velocity at the top of the mixed layer.

The Richardson number of the solution in (35) and (39) is

$$\mathrm{Ri}(y, t) \equiv \frac{b_z}{u_z^2} = \frac{1 - \cos\xi}{\sin^2\xi}. \quad (41)$$

At the equator $\mathrm{Ri}(0, t) = 1/2$ and for a parallel steady flow this indicates stability. However, on the trajectory $y = 2\pi/t$, we have $\mathrm{Ri} = 0$ and presumably stratified shear flow instabilities are possible, although the complicated structure of the unsteady, nonparallel flow in (35) prevents comparison with well-known profiles. However, we can also calculate from (35) and (39) that

$$\int_{-1}^{0} (u_1'^2 + v_1'^2)/2\,dz = \int_{-1}^{0} zb_2\,dz = (\mu^2 t^2/12)\left[\frac{1 - \cos\xi}{\xi^2}\right]. \quad (42)$$

Thus, for the baroclinic fields the vertically integrated kinetic energy density is equal to the vertically integrated potential energy density. In other words the kinetic energy of the baroclinic jet is produced by the local release of potential energy which is just the lowering of the center of mass of the mixed layer as the isopycnals tilt (Fig. 12). (By contrast, the kinetic energy of the Yoshida jet is produced nonlocally by pressure work.) The standard physical explanation of the Richardson number criterion says that a necessary condition for instability is that the kinetic energy density be equal to or greater than the potential energy density. This heuristic principle suggests that the flow in (35) is marginally stable.

The limits of validity of the expansion in (26) are restrictive. Of course when $t \sim \epsilon^{-1} \approx 38$ the velocities ϵu_1, etc. are comparable to the Kelvin wave speed and the advective nonlinearities are no longer small. But there is a much more severe condition imposed by the zonal structure of the basic state. The solution above applies only in a region whose nondimensional zonal extent is $-3.1 < x < 3.1$. When $t \sim 6.2$ (about 10 days) the Kelvin wave generated by the changes in zonal structure at the western boundary of the domain will have propagated across the region of interest. The modification of the Yoshida jet by the arrival of the Kelvin wave (and the long Rossby waves) is a well-understood problem in the context of the reduced gravity model (e.g., Philander 1990). An extension of this analysis to include the effects of stratification is beyond the scope of the present work.

The theory developed in this section is limited to a zonal variation in surface wind stress upsetting the zonal static balance. For completeness, the theory is extended to apply to a horizontally sloped buoyancy gradient that is initially balanced by both zonal and meridional wind stresses (see Appendix). This extended theory allows for the possibility of an initial buoyancy gradient that is asymmetric about the equator. This is a more realistic (although still highly idealized) model of the western equatorial warm pool, which has low salinity water to the west and north in the intertropical convergence zone.

The solution of the extended equations in the Appendix follows much the same lines as the zonal case. There are extra terms in the solution arising from the meridional pressure gradient. We recover the accelerating Yoshida jet and obtain an additional steady part for the vertically averaged velocity. Since the Yoshida

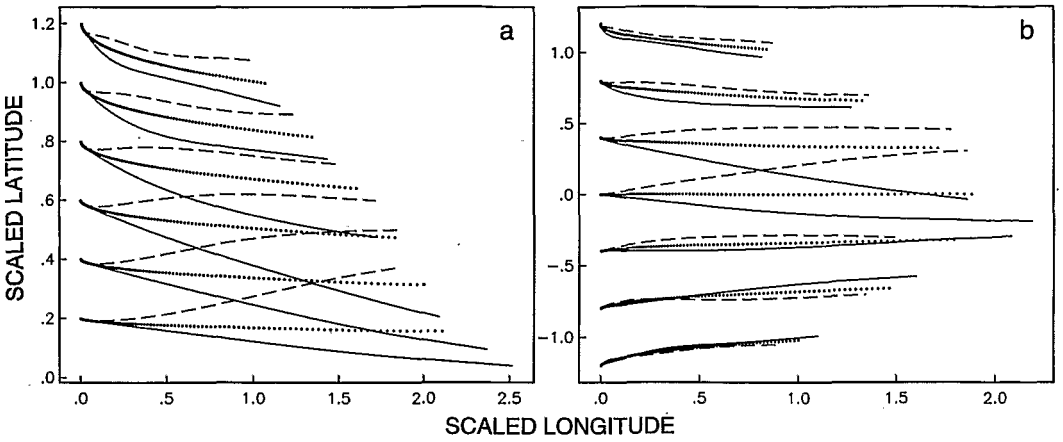

FIG. 14. (a) Float paths at three different depths, surface: $z = 0$ (solid); midlayer: $z = -0.5$ (dots); and base: $z = -1.0$ (dash), obtained by numerical integration of the fresh jet velocity solution that resulted from an upset in a purely zonal balance. The floats were released at a range of latitudes and the resulting tracks are plotted for roughly 16 days. Latitude and longitude are both scaled with the equatorial Rossby radius so 1 unit of latitude or longitude corresponds to 323 km. (b) Same as (a) except unbalanced meridional pressure gradients are also included. The generalized velocity solution is outlined in the Appendix. Note that cross-equatorial flow is produced.

jet dominates at long times, the barotropic velocities are not changed dramatically. However, the sheared part of the velocity is fundamentally different from (35) in that it allows cross-equatorial flow in the active layer. The drifter tracks showed several meridional excursions, along with a tendency to move southward across the equator in early 1992. The zonal theory is unable to model this feature since it is symmetric about the equator. In the next section we trace hypothetical float paths with both unbalanced zonal and meridional pressure gradients. Using realistic values for the initial buoyancy gradients close to the date line, we show that surface floats will initially cross the equator and head southward if the winds are relaxed. Our observations of the barrier layer region and associated sheared jet also show asymmetry about the equator: the jet is centered at 1.5°S in December and shifts north of the equator over the next few months. Meridional wind stress forcing is likely to be partially responsible for these observations and this could be simply included in our generalized theory as outlined in the main text. Based on the calculation in the Appendix, we conclude that meridional pressure gradients offer an explanation for both transequatorial float trajectories and the north–south asymmetry of the jet.

c. *Float displacements in the fresh jet*

It is of interest to trace the path of a hypothetical float released into the fresh jet velocity field. This is calculated by numerically integrating the zonal and meridional velocity solutions while holding the depth constant. In other words, the vertical velocity is ignored so the paths are float tracks rather than particle displacements. We integrated for 10 nondimensional time periods corresponding to a real time period of 16 days. However, as noted in the previous section, the solution begins to lose validity after approximately 10 days.

The tracks for floats released in the velocity fields described by 32 and 35 are plotted in Fig. 14a at three depths in the mixed layer. The midlayer displacements correspond to the Yoshida jet part of the flow. It is clear that the baroclinic velocity forces the float to converge more rapidly toward the equator if it lies above the midpoint of the layer. Zonal velocities increase rapidly close to the equator, so the net effect in the top half of the layer is to significantly increase the total distance traveled by a float. Similarly, the floats in the lower half of the layer diverge away from the equator and are slowed down. With our scaling, unit displacement is equal to 323 km. Surface floats that were initially close to the equator traveled the greatest distance, about 800 km, and reached speeds over 100 cm s^{-1} after about 12 days. At 100 cm s^{-1} a float moves roughly 85 km in one day. These displacements are comparable to those observed (Fig. 10) although obviously our idealized jet cannot reproduce the actual drifter movements.

Our observations showed a fresh jet and associated barrier layer, which was centered south of the equator in late 1991, moving toward the north in early 1992. Additionally, the observed float tracks throughout this time period showed several equatorial crossings. We now show that cross-equatorial flow is produced by the inclusion of unbalanced meridional buoyancy gradients in our simple theory. These more realistic float paths are obtained from the extended velocity fields described in the Appendix. If the initial dynamical balance is purely meridional with no zonal variation, then surface floats will exhibit zonal Ekman transport off the equator

with purely meridional paths as the Coriolis force goes to zero. We modeled the initial buoyancy gradient with both meridional and zonal terms that would approximate the low salinity water to the west and north of the equatorial dateline region. The static balance is upset by the relaxation of the wind.

Float movements in this more realistic velocity field are shown in Fig. 14b. Surface floats released north of the equator head southwards and cross the equator; for example, a float starting at approximately 1°N has crossed the equator in the 16-day time period. The velocity field south of the equator is a result of two competing effects; the convergence toward the equator seen in the previous zonal example and the southward movement responding to the meridional gradient. Near the base of the layer, the tracks cross the equator heading northward. After 16 days, surface floats initially within a degree of the equator have moved approximately 700 km, resulting in a salinity change of approximately 0.2 psu. This is only a fraction of the observed surface salinity anomalies, which reached 1 psu in the center of the fresh jet. The most likely explanation lies with the choice of a linear initial condition instead of a more realistic salinity front. Another simplification is the lack of an arbitrary wind stress distribution in our theory, which we have modeled simply by turning it off resulting in unbalanced pressure gradients.

We expected particle displacements and float displacements to diverge in this complicated velocity field. However, we found that if the float and particle were initially close to the surface then the paths were similar over the time period of interest. Divergence occurs when the starting point is close to the midpoint of the layer. For example, with a midpoint starting depth close to the equator, the endpoints of the float and particle differed by 200 km in longitude and 100 km in latitude after 16 days.

4. Discussion

Having argued that the zonal salinity gradient was significant in driving the 1991–92 eastward jet and consequently in production of the barrier layers, it is worthwhile revisiting the observations of McPhaden et al. (1992). Though westerly wind forcing was clearly present and important in that example, a few aspects of the observations suggest that thermohaline forcing may have also been a factor. First, there was strong shear in the nearly isothermal surface layer, which deepened to about 150 m in thickness. The velocity field had a zero crossing at about 100 m and the velocity and acceleration were westward from 100 m to 150 m. A barrier layer was present, with a step increase in salinity of about 0.2 psu at 50 m and a further increase of about 0.3 psu to the base of the 29°C water. To rationalize this combination of observations solely on the basis of wind forcing requires that the deep westward acceleration be driven by a pressure gradient (downward slope toward the west of the sea surface) with the strong eastward shear toward the surface due to downward diffusion of momentum from the wind. In addition, the presence of the barrier layer suggests that momentum must diffuse downward more efficiently than salt. While this train of logic is not implausible, the fresh jet hypothesis is simpler. In that case, the argument would be that the eastward surface acceleration is due to the sea surface sloping downward to the east. Then, the zonal salinity gradient causes this acceleration to change sign with depth. The presence of the barrier layer is fully consistent with this scenario since diffusion is not required for either salt or momentum. An additional factor in these observations is that the onset of the eastward jet appears to have occurred simultaneously with the relaxation of the trade winds, and several days before the onset of moderate westerlies (McPhaden et al. 1992, Fig. 4). If true, this would imply that the initial slope of the sea surface was indeed downward to the east and could not have caused the westward acceleration at depth. What should be emphasized here is that it may be extremely difficult from the standpoint of observations to distinguish the relative contributions of wind, sea surface slope, and zonal density gradients in driving the jet. None of the datasets collected to date would appear to admit unambiguous interpretation.

A key question with regard to the strong salinity barrier layers seen in the central Pacific is whether these layers may contribute in some way to the air–sea feedbacks, which create and sustain El Niño episodes. Is the barrier layer merely an effect of El Niño or a part of the cause? The speculation by Lukas and Lindstrom (1991) was that barrier layers in the western Pacific may be an important element in the onset of El Niño. The question raised by the present observations is the extent to which the stronger barrier layers seen much farther to the east may contribute to the evolution and eastward propagation of the mature phase.

Measurements of the earth's radiation budget indicate an annually averaged net heating of 60 to 80 W m^{-2} across the Pacific within about 5° of latitude of the equator (Stephens et al. 1981). This heating must be balanced by heat flux divergence in the combined ocean–atmosphere system. The central tropical Pacific Ocean is heated by about 30 W m^{-2}, increasing to greater values in the east and west (Weare et al. 1981). Thus, under mean conditions the equatorial Pacific Ocean absorbs a significant portion of the net radiative heat gain. The principal mechanisms of heat loss in this part of the ocean are zonal and meridional heat advection, and vertical heat diffusion (Enfield 1986). Above the undercurrent core, estimates of vertical turbulent heat flux are as high as 100 W m^{-2} (Peters et al. 1988; Niiler and Stevenson 1982).

The observations discussed in section 2 show that the central equatorial Pacific had, for a period of

months during the mature phase of the 1991–92 El Niño, a strong surface halocline (and pycnocline) within a layer of nearly uniform temperature (>29°C). Because of the uniformity of temperature above and below the strong density gradient, the surface mixed layer could not lose heat downwards. In addition, the anomalous eastward (and possibly meridionally convergent) flow of the equatorial jet removed the horizontal advective contributions to the cooling of the surface layer. Thus, the normal heat balance of the equatorial band was disrupted.

Ramanathan and Collins (1991) found that if the heat absorption in the tropical ocean is small then a radiative equilibrium results in sea surface temperatures around 30°C. At this level of anomalously high sea surface temperatures, the net effect of clouds is to prevent further warming. This is because, as a function of increasing sea surface temperature, the increased reflection of incoming shortwave radiation by cirrus anvils exceeds the greenhouse trapping due to increased cloudiness and atmospheric water vapor. Thus, according to Ramanathan and Collins (1991), a radiative equilibrium exists during El Niños, while during non–El Niño periods the central and eastern Pacific is driven away from radiative equilibrium by ocean heat absorption.

In section 3 we described a dynamical mechanism for production and eastward movement of the salinity barrier layer. By blocking the downward diffusion of heat, this process could plausibly be responsible for switching the system into radiative equilibrium. The initial zonal salinity gradient produces shear in the eastward surface jet. The tilting/shearing mechanism converts the zonal salinity gradient to a vertical salinity gradient in the uniformly warm surface layer, and that surface layer is pushed eastward by the zonal pressure gradient. The mixed layer becomes unmixed in the eastward moving jet, creating an efficient heat trap above the halocline.

This explanation is by no means complete or compelling. The nature and consequences of feedback in the tropical air–sea system are poorly understood. We have examined one physical mechanism in a strongly coupled and complex system. The observations are sparse and the dynamical arguments advanced here are highly simplified. But the problem is thought provoking because the surface barrier layer is a strong signal and each of the ensuing elements of the problem is also of large magnitude. The vertical shear in acceleration is of the same order as the acceleration, which itself balances the zonal pressure gradient. The resulting barrier layers occur in the same narrow equatorial band where normally the heat gain by the ocean is about half the total heat gain by the air–sea column, and where the downward turbulent diffusion can be large. It is plausible that such strong perturbations of the normal balances in the equatorial ocean have additional consequences.

It may seem surprising that the strong surface-layer haloclines described in section 2 have not been extensively documented. The presence of salinity barrier layers in all three tropical oceans, based on historical hydrographic data, was demonstrated by Sprintall and Tomczak (1992). But the regular collection of salinity profiles, except from research vessels, has not been possible prior to the recent advent of the XCTD. Thus, while there have been tens of thousands of temperature profiles collected from merchant vessels in the tropical Pacific over the past few decades and a smaller but still substantial collection of surface salinities, there is a critical lack of subsurface salinity data. Systematic collection of salinity profiles, either from passing ships or long-term moorings, is required over a period of many years, particularly within a few degrees of the equator, to define the spatial scale and evolution of the barrier layer phenomenon.

We have discussed a number of physical processes of potential importance that are not incorporated into current models and theories of ENSO. For instance, while the role of the "slow SST" mode has been emphasized (e.g., Hirst 1988; Neelin 1990), there has been no study of the "slow salinity" mode. The reason for this neglect is understandable: sea surface temperature anomalies have a direct effect on the circulation of the tropical atmosphere (Gill 1980). The role of salinity is more subtle, but perhaps just as important. Another physical process illustrated by the calculation in section 3b, and neglected in current ENSO models, is the tilting and unmixing of the mixed layer by vertically sheared currents. In our calculation the vertical shear is due to horizontal gradients in salinity, but in an analogous way horizontal gradients in mixed-layer temperature must produce vertically sheared velocities that tilt isotherms. In the western Pacific warm pool this effect is small because the horizontal temperature differences are much smaller than the horizontal salinity differences. But over the full zonal extent of the Pacific Ocean tilting due to the zonal temperature gradient must continuously unmix the mixed layer. For example, in the eastern Pacific the thermocline shoals from about 130 m at 140°W to about 50 m at 100°W. If we assume that the temperature drops by 8°C as we pass through the thermocline, and the zonal temperature change in the mixed layer is 5°C then the acceleration is reduced by 50% at the base of the mixed layer. This process is not represented in the standard reduced gravity model in which the pressure forces are due solely to the displacement of the thermocline and are independent of depth.

Acknowledgments. We are most grateful to Blue Star Line, Inc. and to the captains and crews of M/V *Southland Star* for their continued assistance and cooperation. Data processing was carried out by L. Lehmann. P. Sutton and B. Cornuelle participated in data collection. P. Niiler and K. Bi kindly provided drifter

trajectories. The work was supported by the National Science Foundation as a component of the World Ocean Circulation Experiment through Grants OCE87-10084 and OCE90-04230.

APPENDIX

Generalization of the Fresh Jet Model

The restriction to zonal surface winds relaxing or reversing to upset a zonal static balance is unrealistic and unnecessary since meridional variations can easily be incorporated into the theory. We now generalize the model to incorporate a horizontally sloped initial buoyancy gradient. This allows for a buoyancy gradient that is asymmetric about the equator and can therefore crudely model both the zonal salinity front along the equator and the meridional front north of the equator associated with the intertropical convergence zone. As before, we assume an initially static balance between the pressure gradient and the vertical divergence of the Reynolds' stress. The density field when $t < 0$ has the form

$$b = B(1 - \Gamma_B[x\cos\theta_B + y\sin\theta_B]),$$

$$h = H(1 - \Gamma_H[x\cos\theta_H + y\sin\theta_H]). \quad \text{(A1)}$$

The two angles θ_B and θ_H model the horizontal tilt from a meridian of the salinity front and thermocline, respectively. We have already studied the case of a purely zonal negative buoyancy gradient, which corresponds to $\theta_B = 0$. Near the date line at the equator, the buoyancy in the isothermal layer increases toward the north. A typical value of θ_B is approximately $-\pi/3$. At this longitude, the thermocline slopes upwards to the east in response to the moderate trades. There is also a slight thermocline slope across the equator with the thermocline surfacing to the north. Previously, we chose $\theta_H = 0$, but a more realistic value is $\theta_H = \pi/30$. We assume that initially the zonal and meridional gradients of the pressure field are balanced by the stress divergence produced by the mean wind, which is mainly easterly. We now consider the response to a sudden relaxation of both the meridional and zonal winds. This leaves unbalanced zonal and meridional pressure gradients in the active layer.

We proceed as before by nondimensionalizing using the equatorial scalings outlined in the main text. The same small parameters ϵ and μ are introduced. In summary, the generalized nondimensional equations at $t > 0$ are

$$u_t - yv + p_x = 0, \quad \text{(A2a)}$$

$$v_t + yu + p_y = 0, \quad \text{(A2b)}$$

$$-b + p_z = 0, \quad \text{(A2c)}$$

$$u_x + v_y + w_z = 0, \quad \text{(A2d)}$$

$$\frac{Db}{Dt} = 0. \quad \text{(A2e)}$$

As before, the base of the active layer is a material surface and is isolated from interaction with the deep layer, so that

$$\tilde{p} = 0, \quad h_t + \tilde{u}h_x + \tilde{v}h_y + \tilde{w} = 0. \quad \text{(A3)}$$

The nondimensional initial conditions are

$$b = (1 - \epsilon\mu[x\cos\theta_B + y\sin\theta_B]),$$

$$h = (1 - \epsilon\mu^{-1}[x\cos\theta_H + y\sin\theta_H]),$$

$$u_1 = v_1 = w_1 = h_1 = b_1 = 0. \quad \text{(A4)}$$

Expansion of the variables in ϵ gives

$$(u, v, w) = \epsilon(u_1, v_1, w_1) + \epsilon^2(u_2, v_2, w_2) + \cdots$$

$$b = 1 - \epsilon\mu(x\cos\theta_B + y\sin\theta_B) + \epsilon b_1 + \epsilon^2 b_2 + \cdots$$

$$h = 1 - \epsilon\mu^{-1}(x\cos\theta_H + y\sin\theta_H) + \epsilon h_1 + \epsilon^2 h_2 + \cdots$$

$$p = 1 + z + \epsilon[(-\mu\cos\theta_B x - \mu\sin\theta_B y)(1 + z) - \mu^{-1}(\cos\theta_H x + \sin\theta_H y) + h_1] + \cdots. \quad \text{(A5)}$$

The pressure field expansion is once again simplified because $b_{1t} = 0$. The order ϵ balances in the remaining equations of motion are

$$u_{1t} = yv_1 - \mu\cos\theta_B(1 + z) - \mu^{-1}\cos\theta_H + h_{1x} = 0,$$

$$v_{1t} + yu_1 - \mu\sin\theta_B(1 + z) - \mu^{-1}\sin\theta_H + h_{1y} = 0,$$

$$h_{1t} + \bar{u}_{1x} + \bar{v}_{1y} = 0. \quad \text{(A6)}$$

These are the generalized version of (29) in the main text although they do not include meridional or zonal wind stress terms, which are omitted for simplicity. The zonal momentum balance is little changed as the same terms appear but with constants modified by θ_B and θ_H. However, the meridional momentum equations now have additional terms due to the meridional buoyancy gradient. These terms introduce a new part to the velocity solution, which is unlike the Yoshida jet solution. To solve, we proceed as before and vertically integrate the equations. The averaged equations with the zonal derivatives dropped are

$$\bar{u}_{1t} - y\bar{v}_1 = \mu_c,$$

$$\bar{v}_{1t} + y\bar{u}_1 = -h_{1y} + \mu_s,$$

$$h_{1t} + \bar{v}_{1y} = 0, \quad \text{(A7)}$$

where we have combined the constants as $\mu_c = (\mu/2)\times\cos\theta_B + \mu^{-1}\cos\theta_H$ and $\mu_s = (\mu/2)\sin\theta_B + \mu^{-1}\sin\theta_H$. First we note that the equations are linear and that we already have the velocity solutions that correspond to $\mu_s = 0$. This "Yoshida jet" solution is

$$\bar{u}_{11} = \mu_c y^{-1}\mathcal{Q}''(y)t + u_{11}^{\dagger}(y, t), \quad \text{(A8.1)}$$

$$\bar{v}_{11} = \mu_c\mathcal{Q}(y) + v_{11}^{\dagger}(y, t), \quad \text{(A8.2)}$$

$$h_{11} = -\mu_c\mathcal{Q}'(y)t + h_{11}^{\dagger}(y, t), \quad \text{(A8.3)}$$

where the function $\mathcal{Q}(y)$ is the bounded solution of

$$\mathcal{Q}'' - y^2\mathcal{Q} = y. \tag{A9}$$

We do not solve for the oscillatory fields, $u_{11}^{\dagger}(y, t)$, etc., that are excited by the sudden change of wind. The second half of the velocity solution is obtained by letting $\mu_c = 0$. Conservation of potential vorticity implies that

$$\partial_t(yu_y + y^2h - u) = 0. \tag{A10}$$

In fact, from the initial conditions we know that the bracketed quantity is zero. Therefore,

$$yu_y + y^2h - u = 0. \tag{A11}$$

We rearrange (A11) and the steady part of (A8b) to get a time-independent equation in terms of one variable; namely,

$$yh_{yy} - 2h_y - y^3h = -2\mu_s. \tag{A12}$$

Now we introduce a steady function $\mathcal{P}(y)$ such that

$$y\mathcal{P}'' - 2\mathcal{P}' - y^3P = -2. \tag{A13}$$

The second half of the barotropic velocity solution can be written in terms of $\mathcal{P}(y)$ and oscillatory solutions that are excited by the abrupt change in the wind field. We how have

$$\bar{u}_{21} = \mu_s y^{-1}(1 - \mathcal{P}'(y)) + u_{21}^{\dagger}(y, t), \tag{A14a}$$

$$\bar{v}_{21} = 0 + v_{21}^{\dagger}(y, t), \tag{A14b}$$

$$h_{21} = \mu_s\mathcal{P}(y) + h_{21}^{\dagger}(y, t). \tag{A14c}$$

Moore and Philander (1977) give explicit expressions for the oscillatory fields. It is clear that the response of the system to an upset in the meridional momentum balance differs markedly from a zonal dynamical imbalance. There is no accelerating eastward jet in response to a weakening of the trades. The Ekman transport is now seen in the zonal velocity field and the vertically averaged meridional velocity is oscillatory in time. The total barotropic solution is just the superposition of the solutions given by (A8) and (A14). At large times, the "Yoshida jet" solution dominates the zonal velocity solution, so that the barotropic velocities are not remarkably different from those studied in the main text.

We now obtain the baroclinic velocity solutions by subtracting the vertically averaged equations from the full set of equations. The solution with $\mu_s = 0$ is changed only by the multiplicative constant and is

$$u'_{11} = \mu t \cos\theta_B(z + 1/2)\left[\frac{\sin\xi}{\xi}\right]$$

$$v'_{11} = -\mu t \cos\theta_B(z + 1/2)\left[\frac{1 - \cos\xi}{\xi}\right], \tag{A15}$$

where

$$\xi \equiv yt. \tag{A16}$$

Notice that the horizontal thermocline tilt does not affect the sheared velocities, it is only the horizontal tilt in the initial buoyancy gradient, contained in θ_B, that appears in the solution. Next we solve the second part of the solution when $\mu_c = 0$. The horizontal momentum equations are

$$u'_{21t} - yv'_{21} = 0$$

$$v'_{21t} + yu'_{21} = \mu \sin\theta_B(z + 1/2) \tag{A17}$$

with solutions:

$$u'_{21} = \mu t \sin\theta_B(z + 1/2)\left[\frac{1 - \cos\xi}{\xi}\right]$$

$$v'_{21} = \mu t \sin\theta_B(z + 1/2)\left[\frac{\sin\xi}{\xi}\right]. \tag{A18}$$

By linear superposition the total baroclinic solution is the sum of the fields in (A15) and (A18). Vertical shear is produced by the horizontal buoyancy gradient; thermocline slope plays no part. The interesting aspect of the new baroclinic velocities is that v'_{21} is nonzero at the equator and therefore allows for accelerating cross-equatorial flow in the active layer. This is not a feature of the barotropic flow, which is barred from crossing from one hemisphere to another (see A14b). The reader is referred to section 3c of the text for figures displaying tracks of floats released in the total velocity fields given by (A8), (A14a, b), (A15), and (A18).

REFERENCES

Climate Analysis Center, 1991a: Climate diagnostics bulletin, September, 1991. No. 91/9, National Oceanic and Atmospheric Administration. 75 pp.

——, 1991b: Climate diagnostics bulletin, December, 1991. No. 91/12, National Oceanic and Atmospheric Administration. 75 pp.

Donguy, J. R., 1987: Recent advances in the knowledge of the climatic variations in the tropical Pacific Ocean. *Progress in Oceanography,* Vol. 19, Pergamon, 49–85.

——, and A. Morliere, 1983: Bimodal surface salinity states in the western tropical Pacific Ocean. *Tropical Ocean–Atmos. Newslett.,* **18,** 9.

Enfield, D. B., 1986: Zonal and seasonal variations in the near-surface heat balance of the equatorial Pacific. *J. Phys. Oceanogr.,* **16,** 1038–1054.

Firing, E., R. Lukas, J. Sadler, and K. Wyrtki, 1983: Equatorial undercurrent disappears during 1982–1983 El Niño. *Science,* **222,** 1121–1123.

Gill, A. E., 1980: Some simple solutions for heat induced tropical circulation. *Quart. J. Roy. Meteor. Soc.,* **106,** 447–462.

Hirst, A. C., 1988: Slow instabilities in tropical ocean basin–global atmosphere models. *J. Atmos. Sci.,* **45,** 830–852.

Kessler, W., and B. Taft, 1987: Dynamic heights and zonal geostrophic transports in the central tropical Pacific during 1979–84. *J. Phys. Oceanogr.,* **17,** 97–122.

Lukas, R., 1990: The role of salinity in the dynamics and thermodynamics of the western Pacific warm pool. *Proc. Int. TOGA Scientific Conf.,* Honolulu, Hawaii, WCRP-43, WMO/TD No. 379, 73–81.

——, and E. Lindstrom, 1991: The mixed layer of the western equatorial Pacific Ocean. *J. Geophys. Res.*, **96**(Suppl.), 3343–3357.

McPhaden, M., S. Hayes, L. Mangum, and J. Toole, 1990: Variability in the western equatorial Pacific Ocean during the 1986–87 El Niño Southern Oscillation event. *J. Phys. Oceanogr.*, **20**, 190–208.

——, F. Bahr, Y. du Penhoat, E. Firing, S. Hayes, P. Niiler, P. Richardson, and J. Toole, 1992: The response of the western equatorial Pacific Ocean to westerly wind bursts during November 1989 to January 1990. *J. Geophys. Res.*, **97**, 14 289–14 303.

Moore, D. W., and S. G. H. Philander, 1977: Modelling of the tropical ocean circulation. *The Sea,* Vol. 6, E. D. Goldberg, I. N. McCave, J. J. O'Brien, and J. H. Steele, Eds., Wiley Interscience, 319–361.

Neelin, J. D., 1990: A hybrid coupled general circulation model for El Niño studies. *J. Atmos. Sci.*, **47**, 674–693.

Niiler, P., and J. Stevenson, 1982: The heat budget of tropical ocean warm-water pools. *J. Mar. Res.*, **40**(Suppl.), 465–480.

Peters, H., M. Gregg, and J. Toole, 1988: On the parameterization of equatorial turbulence. *J. Geophys. Res.*, **93**, 1199–1218.

Philander, S. G., 1990: *El Niño, La Niña and the Southern Oscillation.* Int. Geophys. Ser., Vol. 46, Academic Press.

Ramanathan, V., and W. Collins, 1991: Thermodynamic regulation of ocean warming by cirrus clouds deduced from observations of the 1987 El Niño. *Nature,* **351**, 27–32.

Sprintall, J., and M. Tomczak, 1992: Evidence of the barrier layer in the surface layer of the tropics. *J. Geophys. Res.*, **97**, 7305–7316.

Stephens, G., G. Campbell, and T. Vonder Haar, 1981: Earth radiation budgets. *J. Geophys. Res.*, **86**, 9739–9760.

Weare, B., T. Strub, and M. Samuel, 1981: Annual mean surface heat fluxes in the tropical Pacific Ocean. *J. Phys. Oceanogr.*, **11**, 705–717.

Wyrtki, K., 1984: The slope of sea level along the equator during the 1982/1983 El Niño. *J. Geophys. Res.*, **89**, 10 419–10 424.

Fresh Equatorial Jets

DEAN ROEMMICH, MICHELE MORRIS, AND W. R. YOUNG

J. R. DONGUY

Reprinted from JOURNAL OF PHYSICAL OCEANOGRAPHY, Vol. 24, No. 3, March 1994
American Meteorological Society